Report

Cell Reports

Plasmodium Para-Aminobenzoate Synthesis and Salvage Resolve Avoidance of Folate Competition and Adaptation to Host Diet

Graphical Abstract

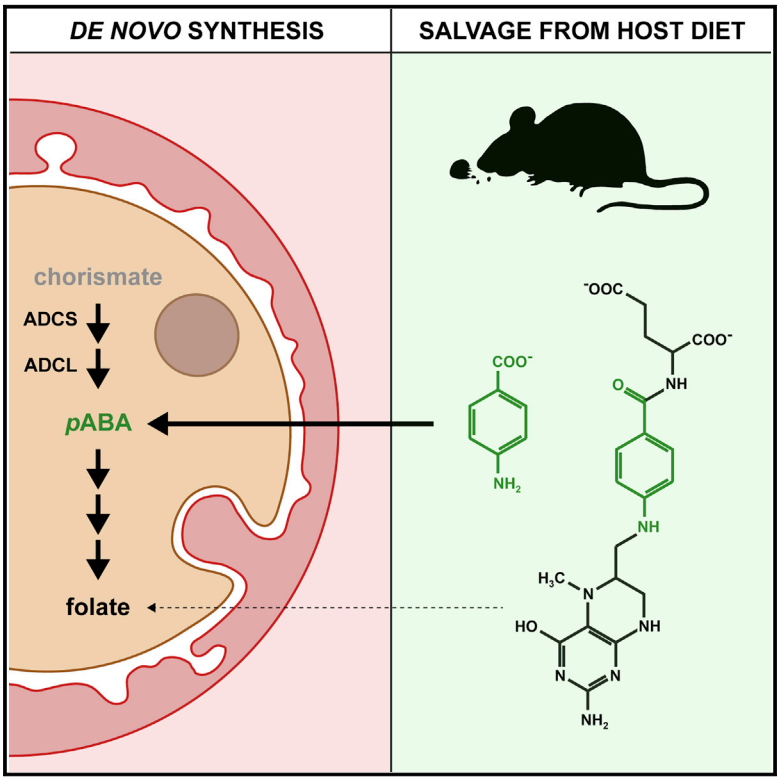

Highlights

- *Plasmodium* parasites harbor their own *p*ABA biosynthesis pathway
- Combined absence of *p*ABA synthesis and salvage is lethal to parasite blood stages
- Import of *p*ABA, not folate, is physiological for blood-stage parasites
- *Plasmodium* exploits alternative folate acquisition during life cycle progression

Authors

Joachim Michael Matz, Mutsumi Watanabe, Mofolusho Falade, Takayuki Tohge, Rainer Hoefgen, Kai Matuschewski

Correspondence

joachim.michael.matz@hu-berlin.de

In Brief

Matz et al. present an integrated approach of experimental genetics and nutritional metabolite restriction to demonstrate two complementary folate acquisition strategies of the malaria parasite in the blood: endogenous synthesis and salvage of the folate precursor *p*ABA. Uptake of *p*ABA, and not folate, is physiological, facilitating avoidance of host-parasite competition.

Matz et al., 2019, Cell Reports *26*, 356–363
January 8, 2019
https://doi.org/10.1016/j.celrep.2018.12.062

CellPress

OPEN ACCESS
CellPress

Cell Reports
Report

Plasmodium Para-Aminobenzoate Synthesis and Salvage Resolve Avoidance of Folate Competition and Adaptation to Host Diet

Joachim Michael Matz,[1,2,6,*] Mutsumi Watanabe,[3,4] Mofolusho Falade,[5] Takayuki Tohge,[3,4] Rainer Hoefgen,[3] and Kai Matuschewski[1,2]

[1]Department of Molecular Parasitology, Institute of Biology, Humboldt University, 10115 Berlin, Germany
[2]Parasitology Unit, Max Planck Institute of Infection Biology, 10117 Berlin, Germany
[3]Department of Molecular Physiology, Max Planck Institute of Molecular Plant Physiology, 14476 Potsdam-Golm, Germany
[4]Nara Institute of Science and Technology, Graduate School of Biological Sciences, Plant Secondary Metabolism, 8916-5 Takayama-cho, Ikoma, Nara 630-0192, Japan
[5]University of Kentucky College of Pharmacy, Lexington, KY, USA
[6]Lead Contact
*Correspondence: joachim.michael.matz@hu-berlin.de
https://doi.org/10.1016/j.celrep.2018.12.062

SUMMARY

Folate metabolism is essential for DNA synthesis and a validated drug target in fast-growing cell populations, including tumors and malaria parasites. Genome data suggest that *Plasmodium* has retained its capacity to generate folates *de novo*. However, the metabolic plasticity of folate uptake and biosynthesis by the malaria parasite remains unresolved. Here, we demonstrate that *Plasmodium* uses an aminodeoxychorismate synthase and an aminodeoxychorismate lyase to promote the biogenesis of the central folate precursor *para*-aminobenzoate (*p*ABA) in the cytoplasm. We show that the parasite depends on *de novo* folate synthesis only when dietary intake of *p*ABA by the mammalian host is restricted and that only *p*ABA, rather than fully formed folate, is taken up efficiently. This adaptation, which readily adjusts infection to highly variable *p*ABA levels in the mammalian diet, is specific to blood stages and may have evolved to avoid folate competition between the parasite and its host.

INTRODUCTION

Malaria parasites replicate at high rates in the mammalian bloodstream. Consequently, they require large quantities of folate and folate precursors, which they scavenge from the serum or synthesize *de novo* (Krungkrai et al., 1989; Müller and Hyde, 2013). In contrast, the mammalian host strictly depends on the dietary uptake of preformed folates. Folates promote essential functions during one-carbon transfer reactions and consist of three major moieties: *para*-aminobenzoate (*p*ABA), pterin, and glutamate. The growth-inhibitory effects of antifolates targeting the enzymes dihydropteroate synthase (DHPS) and dihydrofolate reductase-thymidylate synthase (DHFR-TS) have been exploited for antimalarial therapy (Nzila, 2006). Due to the emergence of antifolate resistance, these enzymes have received considerable attention (Gregson and Plowe, 2005; Heinberg and Kirkman, 2015). For therapeutic approaches, however, the enzymes promoting biogenesis of the central folate precursor *p*ABA have been neglected.

It is believed that chorismate, which is produced via the shikimate pathway (Roberts et al., 1998), is converted to *p*ABA in a two-step reaction (Figure 1A). A potential aminodeoxychorismate synthase (*ADCS*, PBANKA_0823300) and an aminodeoxychorismate lyase (*ADCL*, PBANKA_1322100) are predicted by *Plasmodium* genome sequences (Magnani et al., 2013; Salcedo-Sora and Ward, 2013; Triglia and Cowman, 1999). However, their roles in *Plasmodium* folate metabolism during infection remain unexplored.

Here, we investigate the function of ADCS and ADCL in folate biogenesis. Using a combination of reverse genetics and defined host nutrition, we provide evidence for two complementary pathways: *de novo* biosynthesis and scavenging of *p*ABA. Facultative auxotrophy of *p*ABA during blood infection thus exemplifies the metabolic flexibility of the malaria parasite *in vivo*.

RESULTS AND DISCUSSION

Experimental Genetics of the *p*ABA Synthesis Pathway

We initiated our analysis by assessing *ADCS* and *ADCL* expression throughout the parasite life cycle, using the murine malaria model parasite *P. berghei*. Transgenic parasite lines expressing the endogenous genes fused to mCherry-3xMyc were generated (Figures S1A and S1B) and analyzed by live fluorescence microscopy. Co-localization with a cytosolic GFP marker revealed that both enzymes localize to the parasite cytoplasm (Figure 1B). *ADCS* expression was restricted to blood stage trophozoites and liver stages, but remained below the detection limit in rings, in schizonts, and throughout mosquito infection. This finding indicates distinct roles for *ADCS* in the mammalian host only. In contrast, *ADCL* was ubiquitously expressed during life cycle progression (Figure 1B).

We next assessed the importance of both enzymes by targeted gene disruption and were successful in generating mutants lacking either *ADCS* or *ADCL*, as indicated by diagnostic PCR and Southern blot analysis (Figures 1C, S1C, and S1D).

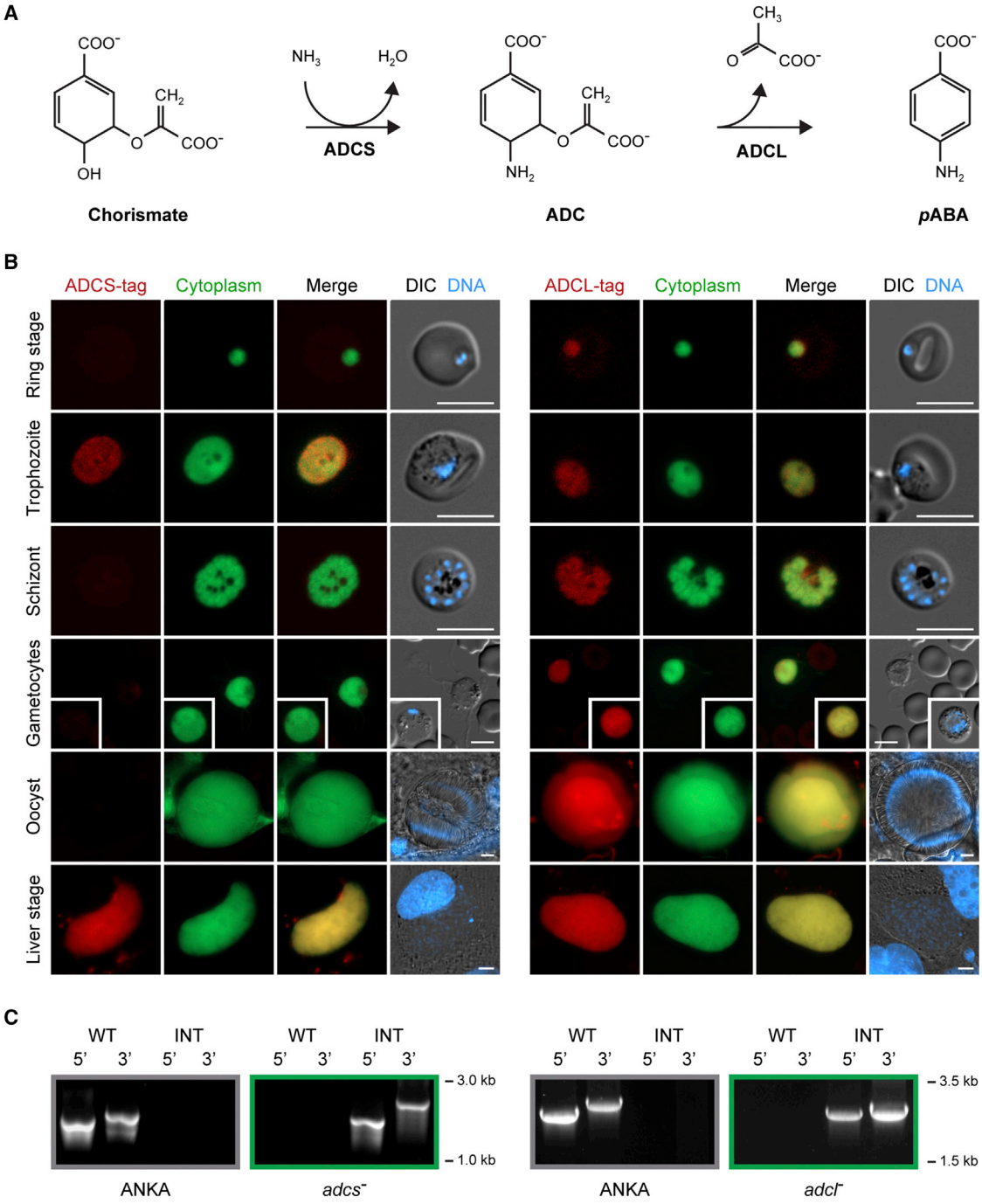

Figure 1. Experimental Genetics of the *Plasmodium* pABA Biosynthesis Pathway

(A) *p*ABA biosynthesis by the malaria parasite. Conversion of chorismate into aminodeoxychorismate (ADC) is catalyzed by ADC synthase (ADCS). ADC is converted into *para*-aminobenzoate (*p*ABA) by ADC lyase (ADCL).

(B) ADCS and ADCL are cytoplasmic proteins. Transgenic *P. berghei* parasites expressing mCherry-3xMyc-tagged ADCS or ADCL and a cytoplasmic GFP marker (Kooij et al., 2012) were passed through the life cycle and imaged live during asexual blood stages, gametogenesis (exflagellating male, egressed female in inset), the mosquito oocyst stage, and the liver stage of infection. Shown are the signals of the tagged proteins (red, left), the cytoplasmic GFP marker (green, center left), a merge of both signals (center right), and a merge of differential interference contrast images (DIC) with Hoechst 33342 nuclear dye (DNA, blue, right). The DNA of male gametocytes was not stained due to interference of the dye with exflagellation. Bars, 5 μm.

(C) Targeted gene deletion of *ADCS* and *ADCL*. Diagnostic PCRs of the WT locus (left) and of the drug-selected and isolated parasites (right) using primer combinations indicated in Figure S1C and Table S1. Green frames indicate successful gene deletion.

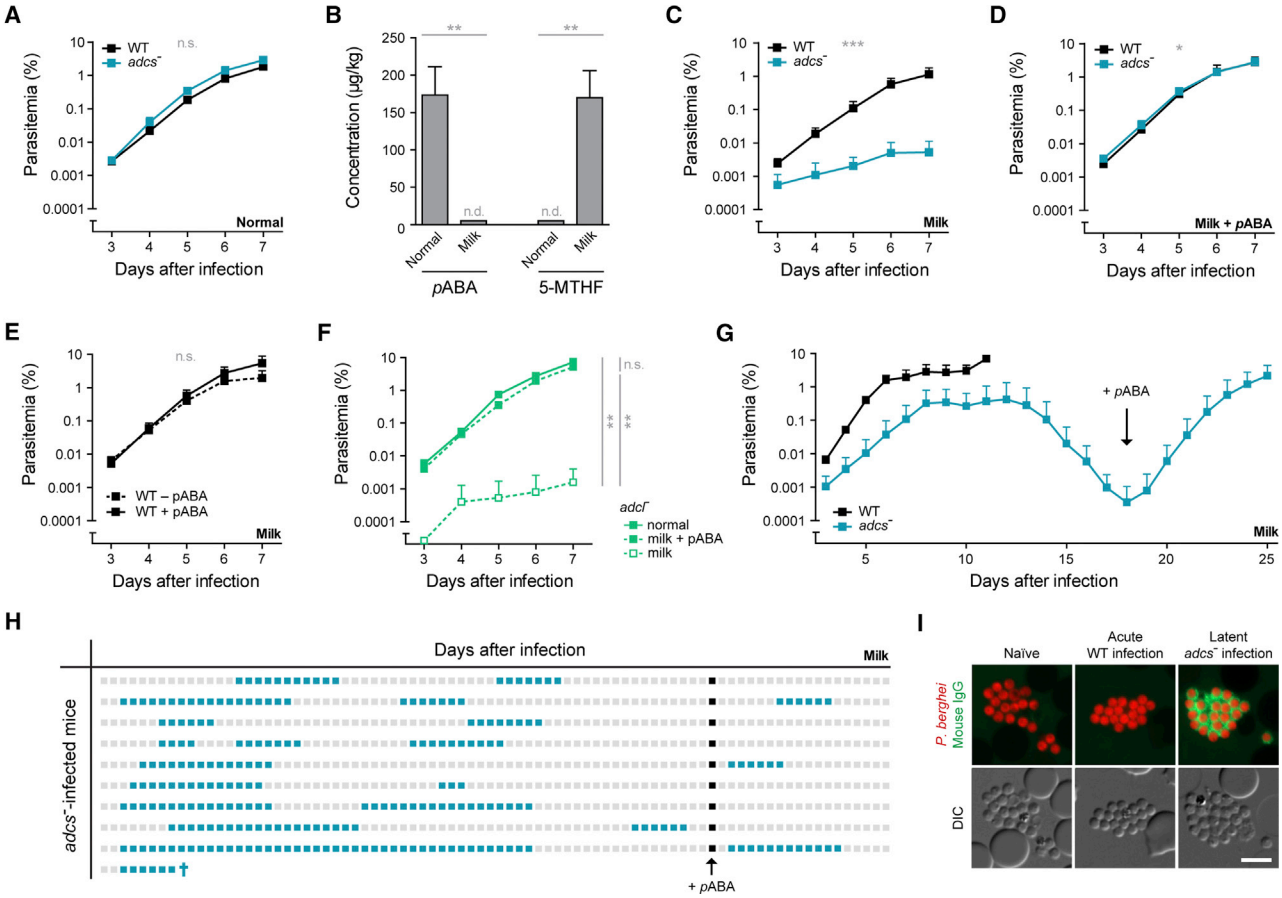

Figure 2. Dietary *p*ABA Restriction Affects *Plasmodium* Parasites Only in the Absence of *ADCS* or *ADCL*

(A) Normal blood stage growth of *adcs*⁻ parasites *in vivo* using a conventional rodent diet. Shown is an intravital competition assay. Equal numbers of mCherry-fluorescent Berred WT and GFP-fluorescent *adcs*⁻ blood stage parasites were co-injected, and peripheral blood was analyzed daily by flow cytometry. n.s., non-significant; analysis of covariance (ANCOVA); n = 4.

(B) Concentrations of *p*ABA and 5-MTHF in conventional rodent diet and milk-based diet. n.d., not detected. **p < 0.01; Student's t test; n = 3. See also Figure S2.

(C and D) Blood stage propagation of WT and *adcs*⁻ parasites was analyzed with an intravital competition assay using a milk-based mouse diet in the absence (C) or presence (D) of dietary *p*ABA. ***p < 0.001; *p < 0.05; ANCOVA; n = 7 (C) or n = 3 (D). Note that the statistical outcome in (D) is due to low variance. See also Figures S1 and S3.

(E) Blood stage development of WT parasites in milk-fed mice in the absence or presence of *p*ABA. n.s., non-significant; ANCOVA; n = 3.

(F) *ADCL*-deficient parasites are also sensitive to dietary *p*ABA restriction. Shown is *adcl*⁻ growth in mice receiving normal or milk-based diet with or without *p*ABA supplementation. **p < 0.001; n.s., non-significant; ANCOVA; n = 5.

(G) Dietary *p*ABA restriction results in declining *adcs*⁻ parasitemia. On day 18, *p*ABA was re-supplied (arrow). WT-infected animals had to be sacrificed due to hyperparasitemia. n = 3 (WT) and 6 (*adcs*⁻). In each panel, mean values ± SDs are shown.

(H) Latent *adcs*⁻ infection and lack of parasite clearance during continued *p*ABA restriction. Shown are 82 days of *adcs*⁻ infection in milk-fed mice. Gray squares, negative; blue squares, positive in Giemsa-stained blood films. On day 65, *p*ABA was re-supplied (arrow). Note the repeated re-emergence of patent blood infection. †, death; n = 10.

(I) Latent *adcs*⁻ infection elicits anti-plasmodial antibodies. Berred WT merozoites (red) were stained with mouse serum and fluorescently labeled secondary anti-mouse immunoglobulin G (IgG) antibodies (green). Sera were derived from naive mice, mice with acute *P. berghei* WT infections (5 days), and from long-term *adcs*⁻-infected mice (H). Bar, 5 µm.

Plasmodium Blood Stages Depend on Host-Derived Nutritional *p*ABA Only upon Loss of Endogenous Synthesis

Blood propagation of *adcs*⁻ parasites was compared to wild-type (WT) in mice fed with conventional rodent diet using an intravital competition assay (Matz et al., 2013). Parasite growth remained unaltered in the absence of *ADCS* (Figure 2A), suggestive of efficient salvage of folate or folate precursors, such as *p*ABA. For this reason, we restricted *p*ABA levels by providing the host with a diet based on spray-dried whole-milk powder. Metabolite quantification by ultra-performance liquid chromatography/Orbitrap-mass spectrometry (UPLC/Orbitrap-MS) confirmed that *p*ABA is abundant in conventional mouse feed and absent from milk diet (Figures 2B and S2B). Moreover, conventional diet is fortified with high levels of the artificial folate analog folic acid (FA), which is absent from milk. In contrast to conventional feed, milk

diet contained considerable levels of the naturally occurring 5-methyltetrahydrofolate (5-MTHF; Figures 2B and S2B). In the liver, *p*ABA is predominantly converted to three derivatives by either acetylation or glycine conjugation (Figure S2A; Song and Hsu, 1996). We measured the levels of two *p*ABA metabolites, *para*-acetamidobenzoate (*p*ACBA) and *para*-aminohippurate (*p*AHA), in the mouse serum. Although *p*AHA remained undetectable, *p*ACBA levels were high only in mice fed with conventional diet (Figure S2C).

In milk-fed mice *adcs*$^{-}$ parasite propagation was severely impaired, whereas WT parasites displayed normal growth (Figure 2C). This suggests that *Plasmodium* can compensate for the absence of dietary *p*ABA by ADCS-dependent *de novo* biosynthesis and that parasite propagation is only arrested in the combined absence of *p*ABA salvage and endogenous synthesis. This phenotype was recapitulated by an independent *adcs*$^{-}$ parasite line lacking the drug-selectable cassette, thus ruling out interference of the DHFR resistance marker (Figures S1C and S1E–S1G). Upon *p*ABA supplementation via the drinking water, *adcs*$^{-}$ growth was fully restored, and mutant parasites grew indistinguishable from WT in milk-fed mice (Figure 2D). Moreover, blood propagation of WT parasites was largely independent of dietary *p*ABA, which is indicative of sufficient rates of *de novo* *p*ABA synthesis (Figure 2E). Our findings are congruent with previous observations that *p*ABA antagonizes the efficacy of antifolate drugs, including sulfadoxine, a structural *p*ABA analog and competitive inhibitor of DHPS (Milhous et al., 1985; Watkins et al., 1985).

We also compared blood infection of transgenic parasites lacking the second *p*ABA synthesis enzyme, ADCL, in mice receiving different diets. *adcl*$^{-}$ parasites also depend on nutritional *p*ABA, demonstrating that both enzymes, ADCS and ADCL, promote *p*ABA biogenesis during blood infection (Figure 2F). The ubiquitous expression of ADCL suggests additional functions, especially during mosquito stages (Figure 1B). A previous study demonstrated a substantial secondary aminotransferase activity of *Plasmodium falciparum* ADCL, which was suggested as contributing to the detoxification of exogenous D-amino acids (Magnani et al., 2013).

We also quantified tagged ADCS by live fluorescence microscopy to test for a potential regulation of expression in the absence of *p*ABA (Figure S3). We demonstrated that steady-state levels of ADCS remain constant irrespective of dietary *p*ABA availability.

Continued *p*ABA restriction led to the retraction of *adcs*$^{-}$ parasitemia from day 12 onward, which was immediately reverted upon addition of *p*ABA on day 18 (Figure 2G). During more extended periods of *p*ABA deficiency, *adcs*$^{-}$ parasitemia dropped below the detection threshold, followed by alternating periods of re-emergence and retraction, indicative of latent malaria infection (Figure 2H). We propose that *adcs*$^{-}$ survival is due to the inefficient utilization of alternate folate sources or to parasite hibernation, as described previously for *P. falciparum* under amino acid-depleted conditions (Babbitt et al., 2012). Upon *p*ABA resupply 2 months later, *adcs*$^{-}$ parasites continued their cycles of emergence and retraction, which is indicative of parasite tolerance rather than sterile protection (Figure 2H).

The persistence of latent infection precludes the combined use of ADCS or ADCL targeting and *p*ABA-free diet as a viable pharmacological strategy or for experimental blood stage immunizations. Our observations also warrant a cautionary note for the development of attenuated blood stage vaccine strains. Although the murine immune system was exposed to large parasite quantities for >80 days, and despite eliciting robust antiparasitic antibodies (Figure 2I), infection with *adcs*$^{-}$ parasites was not resolved, indicating no sterile protection against asexual *P. berghei* blood stages.

Metabolite Profiling Identifies *p*ABA Dependency of *Plasmodium* Blood Stages

*p*ABA supplementation correlated with elevated *p*ACBA levels in the serum, which is indicative of efficient ingestion, resorption, and bioconversion of *p*ABA by the animals (Figures S2C and S2D). Phenotypic rescue of *adcs*$^{-}$ parasites in milk-fed animals was also observed upon supplementation with 5-MTHF (Figure 3A). However, 5-MTHF was rapidly degraded to glutamated *p*ABA (*para*-aminobenzoylglutamate [*p*ABG]) in the drinking water, suggesting that restored *adcs*$^{-}$ growth was due to the uptake of *p*ABA-related degradation products (Figure 3B). Indeed, 5-MTHF supplementation also led to a significant increase in serum *p*ACBA levels (Figures S2C and S2D). Furthermore, it was previously demonstrated that *P. falciparum* can form pteroylpolyglutamate from *p*ABG, which is suggestive of efficient uptake and utilization by the parasite (Krungkrai et al., 1989).

To prevent folate degradation, we used high concentrations of the stable folate analog FA (Figure 3B). *adcs*$^{-}$ growth was not rescued by supplementation with 1.3 mg/kg FA (Figure 3C). Excessive FA concentrations, as found in fortified mouse feed (10 mg/kg), improved blood stage development to a certain degree, but did not fully restore WT-like growth, indicating highly inefficient uptake of folate by the parasite (Figure 3D). This finding is in good agreement with the considerable levels of 5-MTHF naturally occurring in milk diet, which could not sustain efficient *adcs*$^{-}$ parasite growth (Figure 2). Supplementation with FA also led to elevated *p*ACBA levels in the serum (Figures S2C and S2D), indicative of folate catabolism. Since exogenous FA did not restore *adcs*$^{-}$ growth, it is clear that *p*ACBA is not an important substrate for *Plasmodium*. Serum *p*ACBA levels must therefore be regarded as a proxy for efficient metabolite conversion *in vivo*, while the physiological substrate for the parasite remains to be determined. Our metabolic data indicate that *p*ABA and its metabolites rather than folate are salvaged from the host.

We show that *de novo* synthesis and salvage from the serum are complementary strategies, which can each fully satisfy the *p*ABA requirements of the parasite, thus indicating challenges for the therapeutic exploitation of parasite *p*ABA acquisition. We provide evidence that the uptake of folate, as opposed to folate precursors, is of negligible importance for parasite development *in vivo*. Inefficient folate salvage by the parasite is a fundamental prerequisite for the efficacy of antifolate drugs and provides a possible explanation for the inconsistent reports about antifolate treatment failure upon food fortification with FA (Kupka, 2015).

Previous studies report large effects of *p*ABA-free diet on the growth and survival of different non-human primate and rodent

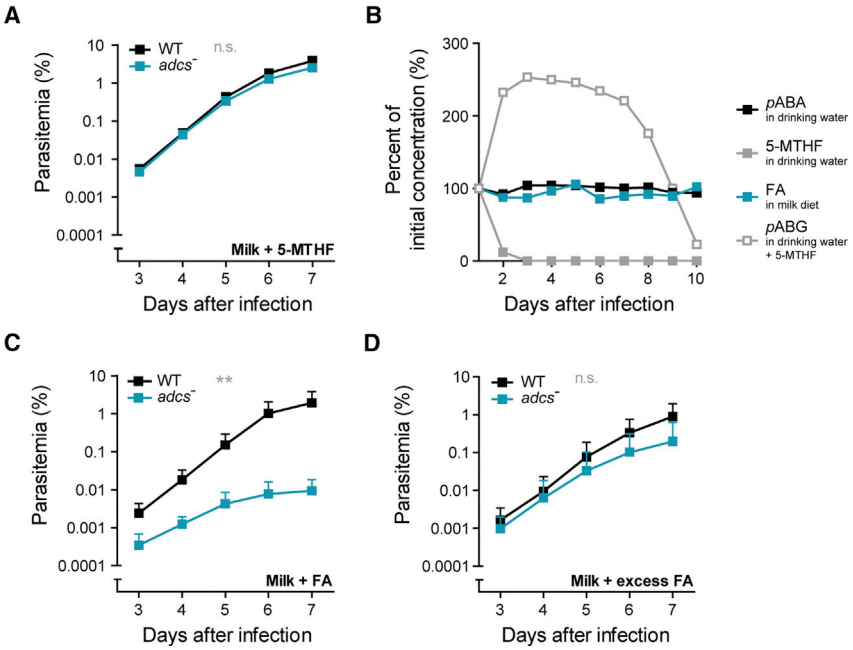

Figure 3. Folate Is a Poor Substrate for the Malaria Parasite during *In Vivo* Infection

(A and B) Degradation of 5-MTHF in the drinking water correlates with the phenotypic rescue of *adcs*⁻ parasites.

(A) Blood stage propagation of WT and *adcs*⁻ parasites was analyzed with the intravital competition assay using milk diet and 5-MTHF-supplemented drinking water.

(B) Stability of food supplements. Concentrations of *p*ABA, 5-MTHF, and FA in drinking water or milk diet. *p*ABG was measured in 5-MTHF-supplemented drinking water. n = 1.

(C and D) Folate is not the preferred substrate of *Plasmodium* parasites *in vivo*. Blood stage propagation of WT and *adcs*⁻ parasites using milk diet supplemented with high (1.3 mg/kg; C) or excessive levels of FA (10 mg/kg; D). Mean values ± SDs are shown. **p < 0.01; n.s., non-significant; ANCOVA; n = 3 (A and C) or n = 6 (D).

See also Figure S2.

malaria parasites, including *P. berghei,* suggestive of a hard-wired metabolic reliance on *p*ABA salvage (Hawking, 1954; Jacobs, 1964; Kicska et al., 2003; Maegraith et al., 1952; Nowell, 1970). In marked contrast, our own results show that WT growth is largely independent of dietary *p*ABA, in good agreement with our experimental genetics data. Growth attenuation was only detected in *adcs*⁻-infected mice when fed on milk diet. We note that we validated dietary *p*ABA restriction by metabolite quantification of the milk diet and the respective mouse sera (Figures 2B and S2B–S2D). We cannot formally exclude that differences in *p*ABA dependency may exist between different *Plasmodium* species, but the discrepancies between our own and previous work with the same murine model parasite *P. berghei* remain puzzling. It was previously noted that the WT growth phenotype in the absence of dietary *p*ABA is rather variable in *P. berghei* mouse infections and may depend on the parasite strain (Nowell, 1970). Contrasting phenotypes could also be attributed to the circumstances of animal husbandry, which are known to influence the composition of the gut microbiome (Franklin and Ericsson, 2017; Rausch et al., 2016). The bacterial community of the digestive tract of the mouse can shape the outcome of malarial infections via a modulation of the animal's inflammatory responses (Villarino et al., 2016). Presumably, previous breeding and rearing conditions differed significantly from today's standards and may thus have affected the microbiota and in consequence the metabolic homeostasis, immune status, and susceptibility of the host toward malaria infection.

Based on our data, we propose that the notion of reduced risk and severity of malaria in breast-fed infants (Brazeau et al., 2016; Murray et al., 1978) cannot be attributed to a *p*ABA-deficient diet but to additional factors, such as slower parasite replication in erythrocytes harboring fetal hemoglobin and the presence of maternal antibodies.

Plasmodium Exploits Alternative Folate Acquisition during Mosquito and Liver Infection

Next, we investigated the contributions of *p*ABA synthesis and salvage during life cycle progression. WT and *adcs*⁻ parasites were co-injected into normally fed mice, allowing for efficient blood stage growth and gametocytogenesis, and were then transmitted to *Anopheles stephensi* mosquitoes in competition. Oocyst and sporozoite numbers remained unaltered in the absence of *ADCS*, independent of *p*ABA supplementation via the mosquito feeding solution (Figures 4A and 4B). We further restricted the carryover of *p*ABA metabolites during the blood meal with the use of milk-fed donor mice. This strategy inevitably led to very low *adcs*⁻ oocyst densities, but it had no effect on growth or sporulation (Figures 4C–4E), suggesting that other folate-related metabolites from the blood meal promote mosquito stage development. Our findings are in perfect agreement with a previous study showing that *P. falciparum* oocyst infection rates and densities are independent of *p*ABA supplementation in *A. stephensi* and *A. gambiae* (Beier et al., 1994). An attractive hypothesis is that folate requirements may be less stringent during the slow replication in the mosquito vector, as opposed to rapid proliferation in the mammalian host.

Next, we inoculated hepatocytes with WT and *adcs*⁻ sporozoites and assessed liver stage development *in vitro*. Cells were grown in *p*ABA-free medium containing dialyzed fetal bovine serum and FA for hepatocyte survival. Parasite morphology, size, and quantity remained unaltered in the absence of *ADCS* and did not improve upon *p*ABA supplementation (Figures 4F and S4). We then assessed intrahepatic growth *in vivo* by injecting sporozoites into milk-fed mice in the absence or presence of dietary *p*ABA. The duration of liver stage development was independent of *ADCS* and *p*ABA, as determined by the time of blood stage patency (Figure 4G). However, quantification of first-generation

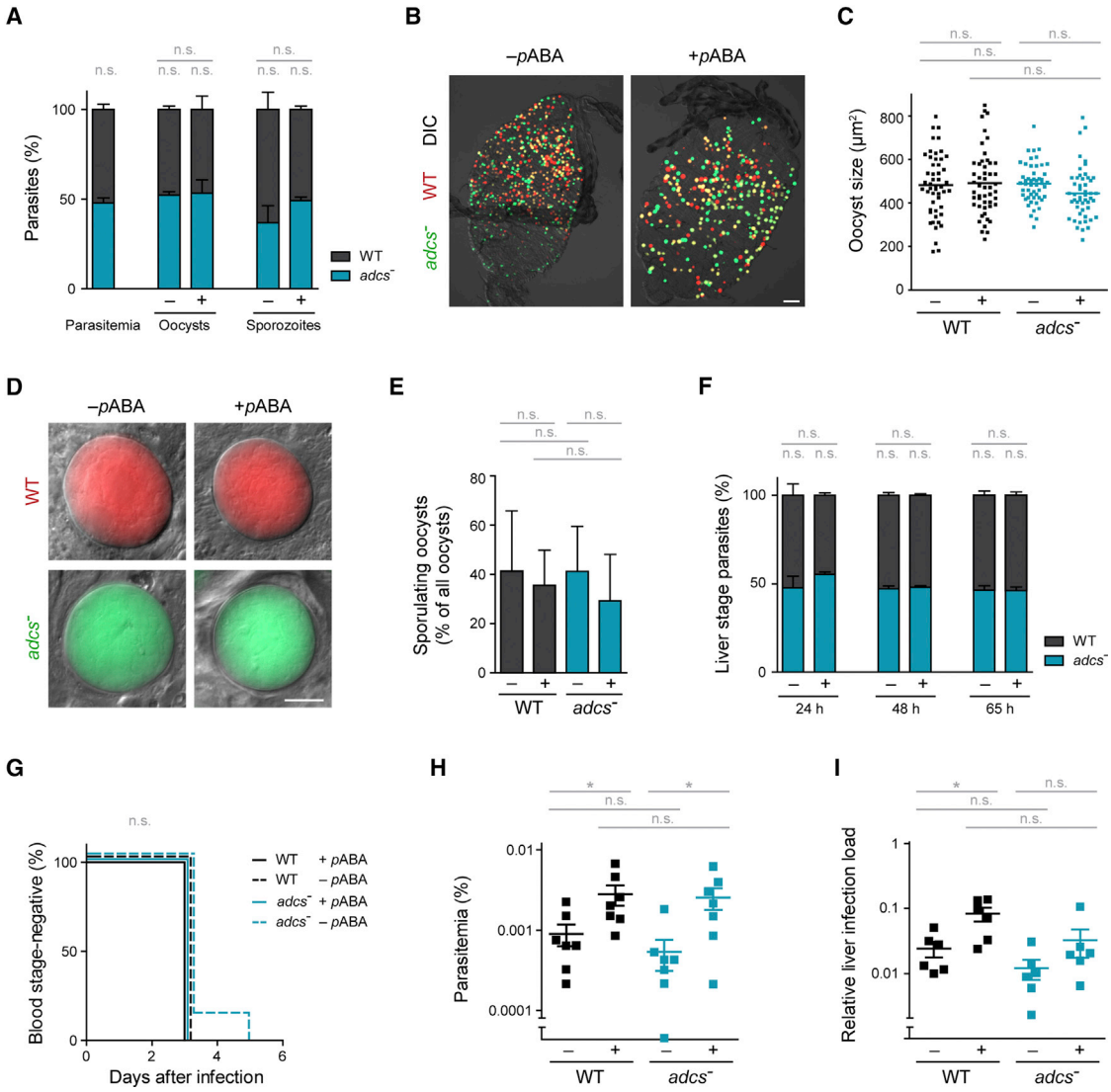

Figure 4. *Plasmodium* Life Cycle Progression Remains Unaltered in the Absence of *ADCS*

(A and B) Normally fed mice were co-injected with equal numbers of mCherry-fluorescent Berred WT and GFP-fluorescent *adcs*⁻ blood stage parasites and fed to *Anopheles stephensi* mosquitoes. + and –, presence or absence of *p*ABA in the mosquito feeding solution.

(A) Quantification of oocysts and sporozoites. Shown is the mean percentage of all single-fluorescent parasites ± SDs. Parasites displaying dual mCherry and GFP fluorescence as a result of cross-fertilization were excluded from analysis. n.s., non-significant; WT versus adcs⁻, paired t test; + versus –, Student's t test; n = 3.

(B) Infected mosquito midguts 10 days after the blood meal. Shown is a merge of mCherry (WT, red), GFP (adcs⁻, green), and differential interference contrast images (DIC). Bar, 100 μm.

(C–E) Normal oocyst maturation in the absence of *ADCS* and *p*ABA. Parasites were transmitted from milk-fed mice to restrict *p*ABA carryover during the blood meal.

(C) Oocyst size on day 11 after the blood meal. Lines, mean values. n.s., non-significant; one-way ANOVA, Tukey's multiple comparison test; n = 50 oocysts from 5 mosquitoes.

(D) Morphology of 11-day-old oocysts. Shown is a merge, as described above. Bar, 10 μm.

(E) Oocyst sporulation on day 14. Mean values ± SDs are shown. n.s., non-significant; one-way ANOVA, Tukey's multiple comparison test; n = 10 infected midguts.

(F) Quantification of liver stage parasites *in vitro*. Hepatoma cells were co-infected with WT and *adcs*⁻ sporozoites and imaged 24, 48, and 65 hr after infection. + and –, presence or absence of *p*ABA in the culture medium. Shown is the mean percentage of all parasites ± SDs. n.s., non-significant; WT versus *adcs*⁻, paired t test; + versus –, Student's t test; n = 3. See also Figure S4.

(G) Time to development of patent blood infection. Milk-fed mice were injected with equal numbers of WT and *adcs*⁻ sporozoites. Peripheral blood was monitored daily by flow cytometry. n.s., non-significant; Mantel-Cox test; n = 7 mice from 3 independent experiments.

(H and I) Beneficial effect of dietary *p*ABA on the first obligate parasite expansion phase in the liver. + and –, presence or absence of *p*ABA in the mouse drinking water.

(legend continued on next page)

blood stage parasitemia and of parasite transcript abundance in infected livers suggests a 3- to 5-fold fitness cost in the absence of *p*ABA, which is indicative of a growth-stimulatory function during liver stage development *in vivo*. The lack of *ADCS* expression caused no significant defects during this stage (Figures 4H and 4I). Since the liver is a major folate pool (Lin et al., 2004), we hypothesize that liver stage survival may be due to the salvage of preformed folates in the absence of *ADCS*. Optimized folate concentrations in the culture medium may thus account for the discrepancies in *p*ABA dependency observed *in vitro* and *in vivo*.

It remains to be determined whether the *p*ABA requirements of human malaria pathogens during intrahepatic growth are comparable to those of *P. berghei*, especially due to their significantly longer development times in the liver. If confirmed by experimental data, then differential requirements of folate building blocks in different host tissues may signify opportunities for stage-specific antimalarial intervention strategies.

Our results reveal critical roles of *Plasmodium ADCS* and *ADCL* in endogenous folate synthesis during food-mediated *p*ABA scarcity in the mammalian host, but facultative *p*ABA auxotrophy is restricted to blood infection. Thus, by using two complementary pathways, *p*ABA salvage and endogenous biosynthesis, *Plasmodium* elegantly solves its metabolic dependence on this central folate precursor. We conclude that the uptake of *p*ABA and its derivatives, and not of folate, promotes blood stage growth *in vivo*. Since *p*ABA is metabolically irrelevant to mammals, its salvage may serve to prevent folate competition between the malaria parasite and its host, thereby significantly contributing to their shared biological fitness.

STAR★METHODS

Detailed methods are provided in the online version of this paper and include the following:

- KEY RESOURCES TABLE
- CONTACT FOR REAGENT AND RESOURCE SHARING
- EXPERIMENTAL MODEL AND SUBJECT DETAILS
  - Mice
  - Mosquitoes
  - Parasites
- METHOD DETAILS
  - Transfection Constructs
  - Recombinant Parasite Lines
  - Live Cell Imaging
  - Metabolite Restriction and Supplementation
  - Metabolite Quantification
  - Blood Stage Development
  - Mosquito Infections
  - Liver Stage Analysis
- QUANTIFICATION AND STATISTICAL ANALYSIS

SUPPLEMENTAL INFORMATION

Supplemental Information includes four figures and one table and can be found with this article online at https://doi.org/10.1016/j.celrep.2018.12.062.

ACKNOWLEDGMENTS

This work was supported in part by the Max Planck Society, Humboldt University, and by the Alliance Berlin Canberra "Crossing Boundaries: Molecular Interactions in Malaria", which is co-funded by a grant from the Deutsche Forschungsgemeinschaft (DFG) for the International Research Training Group (IRTG) 2290 and the Australian National University. M.F. was supported by a fellowship from The World Academy of Sciences-Deutsche Forschungsgemeinschaft (TWAS-DFG). We thank Andreas Kunze and Katrin Kunert for early experiments that led to the present study. We thank Manuel Rauch, Franziska Brückner, Hendrik Grapp, and Änne Michaelis for technical support and Alisdair Fernie for critical reading of the manuscript.

AUTHOR CONTRIBUTIONS

This work was conceived by J.M.M. and K.M. J.M.M. and M.F. performed the *P. berghei* experiments. M.W., T.T., and R.H. performed and analyzed the UPLC/Orbitrap-MS measurements. J.M.M. and K.M. wrote the manuscript with input from all of the authors.

DECLARATION OF INTERESTS

The authors declare no competing interests.

Received: June 19, 2018
Revised: November 26, 2018
Accepted: December 14, 2018
Published: January 8, 2019

REFERENCES

Babbitt, S.E., Altenhofen, L., Cobbold, S.A., Istvan, E.S., Fennell, C., Doerig, C., Llinás, M., and Goldberg, D.E. (2012). *Plasmodium falciparum* responds to amino acid starvation by entering into a hibernatory state. Proc. Natl. Acad. Sci. USA *109*, E3278–E3287.

Beier, M.S., Pumpuni, C.B., Beier, J.C., and Davis, J.R. (1994). Effects of *para*-aminobenzoic acid, insulin, and gentamicin on *Plasmodium falciparum* development in anopheline mosquitoes (Diptera: Culicidae). J. Med. Entomol. *31*, 561–565.

Brazeau, N.F., Tabala, M., Kiketa, L., Kayembe, D., Chalachala, J.L., Kawende, B., Lapika, B., Meshnick, S.R., and Yotebieng, M. (2016). Exclusive breastfeeding and clinical malaria risk in 6-month-old infants: a cross-sectional study from Kinshasa, Democratic Republic of the Congo. Am. J. Trop. Med. Hyg. *95*, 827–830.

Crider, K.S., Bailey, L.B., and Berry, R.J. (2011). Folic acid food fortification-its history, effect, concerns, and future directions. Nutrients *3*, 370–384.

Feldmann, A.M., and Ponnudurai, T. (1989). Selection of *Anopheles stephensi* for refractoriness and susceptibility to *Plasmodium falciparum*. Med. Vet. Entomol. *3*, 41–52.

Franklin, C.L., and Ericsson, A.C. (2017). Microbiota and reproducibility of rodent models. Lab Anim. (NY) *46*, 114–122.

Friesen, J., Silvie, O., Putrianti, E.D., Hafalla, J.C.R., Matuschewski, K., and Borrmann, S. (2010). Natural immunization against malaria: causal prophylaxis with antibiotics. Sci. Transl. Med. *2*, 40ra49.

(H) First-generation parasitemias on day 3 after WT and *adcs*$^{-}$ co-infection. n.s., non-significant; *p < 0.05; WT versus adcs^{-}, paired t test; + versus −, Student's t test; n = 7 mice from 3 independent experiments.
(I) Parasite loads of mouse livers infected with WT or *adcs*$^{-}$, as determined by quantitative real-time PCR using primers indicated in Table S1. n.s., non-significant; *p < 0.05; one-way ANOVA, Tukey's multiple comparison test; n = 6. Mean values ± SEMs are shown.

Giavalisco, P., Li, Y., Matthes, A., Eckhardt, A., Hubberten, H.-M., Hesse, H., Segu, S., Hummel, J., Köhl, K., and Willmitzer, L. (2011). Elemental formula annotation of polar and lipophilic metabolites using (13) C, (15) N and (34) S isotope labelling, in combination with high-resolution mass spectrometry. Plant J. *68*, 364–376.

Gregson, A., and Plowe, C.V. (2005). Mechanisms of resistance of malaria parasites to antifolates. Pharmacol. Rev. *57*, 117–145.

Hawking, F. (1954). Milk, *p*-aminobenzoate, and malaria of rats and monkeys. BMJ *1*, 425–429.

Heinberg, A., and Kirkman, L. (2015). The molecular basis of antifolate resistance in *Plasmodium falciparum*: looking beyond point mutations. Ann. N.Y. Acad. Sci. *1342*, 10–18.

Jacobs, R.L. (1964). Role of *p*-aminobenzoic acid in *Plasmodium berghei* infection in the mouse. Exp. Parasitol. *15*, 213–225.

Janse, C.J., Franke-Fayard, B., Mair, G.R., Ramesar, J., Thiel, C., Engelmann, S., Matuschewski, K., van Gemert, G.J., Sauerwein, R.W., and Waters, A.P. (2006). High efficiency transfection of *Plasmodium berghei* facilitates novel selection procedures. Mol. Biochem. Parasitol *145*, 60–70.

Kenthirapalan, S., Waters, A.P., Matuschewski, K., and Kooij, T.W.A. (2012). Flow cytometry-assisted rapid isolation of recombinant *Plasmodium berghei* parasites exemplified by functional analysis of aquaglyceroporin. Int. J. Parasitol. *42*, 1185–1192.

Kicska, G.A., Ting, L.-M., Schramm, V.L., and Kim, K. (2003). Effect of dietary *p*-aminobenzoic acid on murine *Plasmodium yoelii* infection. J. Infect. Dis. *188*, 1776–1781.

Kooij, T.W.A., Rauch, M.M., and Matuschewski, K. (2012). Expansion of experimental genetics approaches for *Plasmodium berghei* with versatile transfection vectors. Mol. Biochem. Parasitol. *185*, 19–26.

Krungkrai, J., Webster, H.K., and Yuthavong, Y. (1989). *De novo* and salvage biosynthesis of pteroylpentaglutamates in the human malaria parasite, *Plasmodium falciparum*. Mol. Biochem. Parasitol. *32*, 25–37.

Kupka, R. (2015). The role of folate in malaria - implications for home fortification programmes among children aged 6-59 months. Matern. Child Nutr. *11*, 1–15.

Lin, Y., Dueker, S.R., Follett, J.R., Fadel, J.G., Arjomand, A., Schneider, P.D., Miller, J.W., Green, R., Buchholz, B.A., Vogel, J.S., et al. (2004). Quantitation of *in vivo* human folate metabolism. Am. J. Clin. Nutr. *80*, 680–691.

Maegraith, B.G., Deegan, T., and Jones, E.S. (1952). Suppression of malaria (*P. berghei*) by milk. BMJ *2*, 1382–1384.

Magnani, G., Lomazzi, M., and Peracchi, A. (2013). Completing the folate biosynthesis pathway in *Plasmodium falciparum*: *p*-aminobenzoate is produced by a highly divergent promiscuous aminodeoxychorismate lyase. Biochem. J. *455*, 149–155.

Matz, J.M., and Kooij, T.W.A. (2015). Towards genome-wide experimental genetics in the *in vivo* malaria model parasite *Plasmodium berghei*. Pathog. Glob. Health *109*, 46–60.

Matz, J.M., Matuschewski, K., and Kooij, T.W.A. (2013). Two putative protein export regulators promote *Plasmodium* blood stage development *in vivo*. Mol. Biochem. Parasitol. *191*, 44–52.

Milhous, W.K., Weatherly, N.F., Bowdre, J.H., and Desjardins, R.E. (1985). *In vitro* activities of and mechanisms of resistance to antifol antimalarial drugs. Antimicrob. Agents Chemother. *27*, 525–530.

Müller, I.B., and Hyde, J.E. (2013). Folate metabolism in human malaria parasites–75 years on. Mol. Biochem. Parasitol. *188*, 63–77.

Murray, M.J., Murray, A.B., Murray, N.J., and Murray, M.B. (1978). Diet and cerebral malaria: the effect of famine and refeeding. Am. J. Clin. Nutr. *31*, 57–61.

Nakabayashi, H., Taketa, K., Miyano, K., Yamane, T., and Sato, J. (1982). Growth of human hepatoma cells lines with differentiated functions in chemically defined medium. Cancer Res. *42*, 3858–3863.

Nowell, F. (1970). The effect of a milk diet upon *Plasmodium berghei, Nuttallia* (=*Babesia*) *rodhaini* and *Trypanosoma brucei* infections in mice. Parasitology *61*, 425–433.

Nzila, A. (2006). The past, present and future of antifolates in the treatment of *Plasmodium falciparum* infection. J. Antimicrob. Chemother. *57*, 1043–1054.

Rausch, P., Basic, M., Batra, A., Bischoff, S.C., Blaut, M., Clavel, T., Gläsner, J., Gopalakrishnan, S., Grassl, G.A., Günther, C., et al. (2016). Analysis of factors contributing to variation in the C57BL/6J fecal microbiota across German animal facilities. Int. J. Med. Microbiol. *306*, 343–355.

Roberts, F., Roberts, C.W., Johnson, J.J., Kyle, D.E., Krell, T., Coggins, J.R., Coombs, G.H., Milhous, W.K., Tzipori, S., Ferguson, D.J., et al. (1998). Evidence for the shikimate pathway in apicomplexan parasites. Nature *393*, 801–805.

Salcedo-Sora, J.E., and Ward, S.A. (2013). The folate metabolic network of *Falciparum* malaria. Mol. Biochem. Parasitol. *188*, 51–62.

Schindelin, J., Arganda-Carreras, I., Frise, E., Kaynig, V., Longair, M., Pietzsch, T., Preibisch, S., Rueden, C., Saalfeld, S., Schmid, B., et al. (2012). Fiji: an open-source platform for biological-image analysis. Nat. Methods *9*, 676–682.

Schneider, C.A., Rasband, W.S., and Eliceiri, K.W. (2012). NIH Image to ImageJ: 25 years of image analysis. Nat. Methods *9*, 671–675.

Schwach, F., Bushell, E., Gomes, A.R., Anar, B., Girling, G., Herd, C., Rayner, J.C., and Billker, O. (2015). *PlasmoGEM*, a database supporting a community resource for large-scale experimental genetics in malaria parasites. Nucleic Acids Res. *43*, D1176–D1182.

Song, D.J., and Hsu, K.Y. (1996). Determination of *p*-aminobenzoic acid and its metabolites in rabbit plasma by high-performance liquid chromatography with fluorescence detection. J. Chromatogr. B Biomed. Appl. *677*, 69–75.

Triglia, T., and Cowman, A.F. (1999). *Plasmodium falciparum*: a homologue of *p*-aminobenzoic acid synthetase. Exp. Parasitol. *92*, 154–158.

Villarino, N.F., LeCleir, G.R., Denny, J.E., Dearth, S.P., Harding, C.L., Sloan, S.S., Gribble, J.L., Campagna, S.R., Wilhelm, S.W., and Schmidt, N.W. (2016). Composition of the gut microbiota modulates the severity of malaria. Proc. Natl. Acad. Sci. U.S.A. *113*, 2235–2240.

Watkins, W.M., Sixsmith, D.G., Chulay, J.D., and Spencer, H.C. (1985). Antagonism of sulfadoxine and pyrimethamine antimalarial activity *in vitro* by *p*-aminobenzoic acid, *p*-aminobenzoylglutamic acid and folic acid. Mol. Biochem. Parasitol. *14*, 55–61.

STAR★METHODS

KEY RESOURCES TABLE

REAGENT or RESOURCE	SOURCE	IDENTIFIER
Antibodies		
Alexa Fluor® 488-coupled goat anti-mouse IgG	Thermo Fisher Scientific	Cat# A11029; RRID: AB_2534088
Biological Samples		
NMRI mouse sera from long term *adcs*$^{-}$ infections (9x)	This study	N/A
NMRI mouse serum from short term WT infection (1x)	This study	N/A
NMRI mouse serum from naive animal (1x)	This study	N/A
Chemicals, Peptides, and Recombinant Proteins		
para-aminobenzoic acid (*p*ABA)	Sigma-Aldrich	Cat# A9878
para-aminohippuric acid (*p*AHA)	Sigma-Aldrich	Cat# A1422
para-acetamidobenzoic acid (*p*ACBA)	Sigma-Aldrich	Cat# 133337
para-aminobenzoylglutamic acid (*p*ABG)	Sigma-Aldrich	Cat# PHR1334
5-methyltetrahydrofolic acid (5-MTHF), disodium salt	Sigma-Aldrich	Cat# M0132
Folic acid (FA)	Sigma-Aldrich	Cat# F7876
Pyrimethamine	MP Biomedicals	Cat# 0219418025
5-Fluorocytosine	Sigma-Aldrich	Cat# F7129
TRIzol Reagent	Thermo Fisher Scientific	Cat# 15596018
Critical Commercial Assays		
Human T Cell Nucleofector™ Kit	Lonza	Cat# VPA-1002
PCR DIG Probe Synthesis Kit	Roche	Cat# 11636090910
DIG Luminescent Detection Kit	Roche	Cat# 11363514910
RETROscript® Kit	Thermo Fisher Scientific	Cat# AM1710
Power SYBR Green PCR Master Mix	Thermo Fisher Scientific	Cat# 4368577
Experimental Models: Cell Lines		
Homo sapiens (male) hepatoma cell line HuH-7	Nakabayashi et al., 1982; originally obtained from Prof. Dr. Ralf Bartenschlager, Heidelberg University Hospital, Heidelberg, D	HuH-7
Experimental Models: Organisms/Strains		
Plasmodium berghei strain ANKA	Janse et al., 2006; originally obtained from Dr. Chris J. Janse, LUMC, Leiden, NL	Reference clone 15cy1
Plasmodium berghei strain Bergreen	Kooij et al., 2012; generated in own lab	N/A
Plasmodium berghei strain Berred	Matz et al., 2013; generated in own lab	N/A
Plasmodium berghei strain *adcs*$^{-}_{res.}$	This study	N/A
Plasmodium berghei strain *adcs*$^{-}_{sens.}$	This study	N/A
Plasmodium berghei strain *adcl*$^{-}$	This study	N/A
Plasmodium berghei strain *adcs-tag*	This study	N/A
Plasmodium berghei strain *adcl-tag*	This study	N/A
Mus musculus strain Crl:NMRI(Han)	Charles River	Strain Code 605
Mus musculus strain C57BL/6NCrl	Charles River	Strain Code 027
Anopheles stephensi strain Sind-Kasur	Feldmann and Ponnudurai, 1989; originally obtained from Prof. Dr. Robert Sauerwein, Radboudumc, Nijmegen, NL; continued breeding in own facilities	N/A
Oligonucleotides		
See Table S1	N/A	N/A

(*Continued on next page*)

Continued

REAGENT or RESOURCE	SOURCE	IDENTIFIER
Recombinant DNA		
pBAT vector	Kooij et al., 2012; generated in own lab	N/A
ADCS knockout plasmid	This study	N/A
ADCL knockout plasmid	PlasmoGEM	PbGEM-539091
ADCS tagging plasmid	This study	N/A
ADCL tagging plasmid	This study	N/A
Software and Algorithms		
GraphPad Prism®	GraphPad Software	Version 5.03
FIJI	Schindelin et al., 2012; Schneider et al., 2012.	Versions continuously updated
Xcalibur™	Thermo Fisher Scientific	Version 4.1.31.9
Other		
Fortified rodent diet	Ssniff	Cat# V1534-300
Whole milk powder (26% fat)	Saliter	N/A
Fetal Bovine Serum, dialyzed, US origin, One Shot	Thermo Fisher Scientific	Cat# A3382001
Nucleofector™ 2b Device	Lonza	Cat# AAB-1001
StepOnePlus™ Real-Time PCR System	Thermo Fisher Scientific	Cat# 4376600
Acquity UPLC I-Class System	Waters	N/A
Acquity UPLC HSS T3 VanGuard Pre-column, 100Å, 1.8 μm, 2.1 mm X 5 mm,	Waters	Cat# 186003976
Acquity UPLC HSS T3 Column, 100Å, 1.8 μm, 2.1 mm X 100 mm	Waters	Cat# 186003539
Exactive Orbitrap Mass Spectrometer	Thermo Fisher Scientific	Cat# IQLAAEGAAPFALGMBCA

CONTACT FOR REAGENT AND RESOURCE SHARING

Further information and requests for resources and reagents should be directed to and will be fulfilled by the Lead Contact, Joachim Michael Matz (joachim.michael.matz@hu-berlin.de).

EXPERIMENTAL MODEL AND SUBJECT DETAILS

Mice

This study was carried out in strict accordance with the German 'Tierschutzgesetz in der Fassung vom 22. Juli 2009' and the Directive 2010/63/EU of the European Parliament and Council 'On the protection of animals used for scientific purposes'. The protocol was approved by the ethics committee of the Berlin state authority ('Landesamt für Gesundheit und Soziales Berlin', permit number G0294/15).

C57BL/6NCrl mice were used for sporozoite infections. All other parasite infections were conducted with Crl:NMRI(Han) mice. Experimental groups consisted of 8-12 weeks old female litter mates, which were housed together in groups of 3 to 6 animals in filter top cages (Tecniplast, Buguggiate, Italy). The cages were bedded with aspen wood chips (LTE E-002, Abedd, Vienna, Austria) and enriched with plastic tunnels (Ehret, Emmendingen, Germany). Mice were kept at room temperature under a 12 h light / 12 h dark cycle at a constant relative humidity of 45%. For information regarding mouse diet, see Method Details.

Mosquitoes

A. stephensi larvae were reared in water containing 0.1% NaCl and were fed with dry cat food pellets (Brekkies, Affinity Petcare S.A, Barcelona, Spain). 200-400 pupae were collected per mosquito cage. Infected mice were fed to the adult mosquitoes 7-10 days after hatching. For information regarding mosquito feeding solutions, see Method Details.

Parasites

All parasite strains used in this study are derived from transfection of *P. berghei* ANKA cl15cy1. For more information on parasite infections, see Method Details.

METHOD DETAILS

Transfection Constructs

Constructs for endogenous tagging of *ADCS* and *ADCL* with mCherry-3xMyc were designed for single homologous integration (Figure S1A). The sequences directly upstream of the stop codons were amplified from genomic DNA (1,053 and 1,663 bp, respectively) and inserted into the pBAT vector (Kooij et al., 2012) using HpaI in combination with EcoRI or NgoMIV. For the generation of the *ADCS* deletion construct, the 3′ fragment of the gene was amplified from genomic DNA (1,185 bp) and cloned into the pBAT vector using the XhoI and KpnI restriction sites. Subsequently, the 5′ fragment (508 bp) was amplified and cloned into the intermediate vectors using SacII in combination with HpaI. Prior to transfection, the *ADCS* knockout vector was linearized with SalI. Deletion of *ADCL* was performed with the respective NotI-digested *PlasmoGEM* vector (Schwach et al., 2015). Internal restriction sites were used for linearization of the tagging vectors.

Recombinant Parasite Lines

We used advanced experimental genetic techniques to generate all recombinant parasite lines (Matz and Kooij, 2015). Purified WT schizonts were transfected with 5 μg DNA using the Nucleofector™ 2b Device and the Human T Cell Nucleofector™ Kit (Lonza, Basel, Switzerland; Janse et al., 2006). Transfected parasites were injected intravenously into naive NMRI mice, and selected *in vivo* with pyrimethamine-containing drinking water (70 mg/l; MP Biomedicals, Santa Ana, CA, USA). Isogenic *ADCS* knockout mutants were isolated by fluorescence-activated cell sorting (Kenthirapalan et al., 2012). *ADCL*-deficient parasites were cloned by limiting dilution.

To validate correct integration of the transfection vectors and absence of remaining WT parasites, primer combinations were used as indicated in Figures S1A and S1C and Table S1. Southern blot analysis using the PCR DIG Probe Synthesis kit and the DIG Luminescent Detection kit (Roche, Rotkreuz, Switzerland) was performed according to the manufacturer's instructions to confirm the correct genotype of the *adcs*$^{-}$ parasite line. The probe was amplified with primers that were used to generate the 5′ integration sequence of the *ADCS* deletion construct (see Table S1) and hybridized to XmnI restriction-digested genomic DNA.

The *adcs*$^{-}$ parasites were also subjected to *in vivo* negative selection with 5-Fluorocytosine-containing drinking water (1 g/l; Sigma-Aldrich, St. Louis, MO, USA) and to subsequent cloning by limiting dilution. Loss of the drug-selectable cassette was confirmed by diagnostic PCR using the primer combinations indicated in Figure S2C.

Live Cell Imaging

In order to assess protein expression, transgenic parasites expressing mCherry-3xMyc-tagged proteins were passed through the parasite life cycle and imaged live. Fluorescence imaging was performed with a Zeiss AxioObserver Z1 epifluorescence microscope equipped with a Zeiss AxioCam MRm camera (Zeiss, Oberkochen, Germany).

For the detection of anti-parasitic antibodies, 0.5 to 1 mL of blood was collected by cardiac puncture and cellular components and serum were separated by centrifugation. Sera of *adcs*$^{-}$-infected mice were pooled. Immunofluorescence analysis was performed at room temperature by incubating live Berred WT-infected erythrocytes in 100% mouse serum containing 1:500 Alexa Fluor® 488-coupled goat anti-mouse IgG (Life Technologies, Carlsbad, CA, USA) for one hour.

During quantitative assessment of *ADCS* expression, the GFP-fluorescent Bergreen WT reference strain was used as a negative control (Kooij et al., 2012). Microscope settings and exposure times were kept constant to ensure comparability. Signal intensities and parasite sizes were analyzed using FIJI with the appropriate plugins (Schindelin et al., 2012; Schneider et al., 2012).

Metabolite Restriction and Supplementation

Mice were fed *ad libitum* with conventional fortified rodent diet (V1534-300, ssniff, Soest, Germany), or with a diet based on spray-dried whole milk powder (Saliter, Obergrünzburg, Germany). Milk powder was mixed with water, formed into pellets and dried at 60 to 80°C. Mice readily accepted the diet. For phenotypic rescue experiments, drinking water was supplemented with 20 mg/l *p*ABA (Sigma-Aldrich) or equimolar concentrations of 5-MTHF (Sigma-Aldrich). Due to low water solubility, 1.3 mg/kg or 10 mg/kg FA (Sigma-Aldrich) was added to the milk powder. The concentration of 1.3 mg/kg is in the range of the FA levels used in the United States food fortification program (Crider et al., 2011) and exceeds the endogenous 5-MTHF levels of the milk diet by eight times (Figure 2B).

For growth analysis, mice were given different diets, starting two days before parasite injection. For metabolite quantification of mouse sera, naive animals were given different diets for seven days.

Throughout mosquito infection, the feeding solution contained 10% sucrose and either none or 0.05% *p*ABA. During liver stage analysis, cells were grown in Dulbecco's Modified Eagle Medium (DMEM), containing 10% dialyzed fetal bovine serum (Thermo Fisher Scientific, Waltham, USA) with or without 5 mg/l *p*ABA.

Metabolite Quantification

Mouse sera, supplemented drinking water, and diet were stored at −80°C prior to metabolite extraction. 200 μl of frozen mouse serum were homogenized in 800 μl of 100% methanol by using a mixer mill with a zirconia bead for 1 minute at 20 Hz. The extract was sonicated for 10 minutes at 4°C. Afterward, the sample was centrifuged at 20,000 *g* for 10 minutes at 4°C. Supernatants were

dried overnight in a speed vacuum concentrator. The dried sample was dissolved in 150 μl of 80% methanol followed by centrifugation as described above.

35 mg of ground milk pellets and conventional mouse diet were homogenized in 350 μl of 80% methanol followed by centrifugation and extraction as above. Food and serum extracts were spiked with 5 μg/ml isovitexin. Drinking water samples were centrifuged and processed as above.

UPLC/Orbitrap-MS analysis for folate-related metabolites was performed as described previously (Giavalisco et al., 2011). For UPLC separation, 5 μl of the sample were injected into an Acquity UPLC I-Class system equipped with an HSS T3 VanGuard pre-column and an HSS T3 column (Waters, Milford, MA, USA; see also Key Resources Table). Mobile phases were 0.1% formic acid in water and 0.1% formic acid in acetonitrile. Mass spectra were acquired using an Exactive^{TM} Orbitrap mass spectrometer (Thermo Fisher Scientific). *p*ABA, *p*AHA, *p*ACBA, *p*ABG, 5-MTHF and FA were identified and quantified by high resolution *m/z* detection using data obtained by co-elution profile of the respective standard compounds (Sigma Aldrich). Data were analyzed using Xcalibur (version 4.1.31.9, Thermo Fisher Scientific).

Blood Stage Development

Blood stage development was assessed using the previously described intravital competition assay (Matz et al., 2013). In short, 500 mCherry-fluorescent Berred WT and 500 GFP-fluorescent *adcs*$^{-}$ blood stage parasites were co-injected intravenously into NMRI mice. For single infections with WT, *adcs*$^{-}$ or *adcl*$^{-}$, 1,000 blood stage parasites were injected. Parasitemia was analyzed daily by flow cytometry or by microscopic analysis of Giemsa-stained thin blood films.

Mosquito Infections

To test parasite performance during mosquito infection normally fed NMRI mice were co-injected intravenously with $5x10^6$ Berred WT and $5x10^6$ *adcs*$^{-}$ blood stage parasites and fed to *A. stephensi* mosquitoes three days later. Prior to feeding parasitemias of donor mice were measured using flow cytometry. Oocysts and sporozoites were visualized and quantified by live fluorescence microscopy. In order to restrict the carry-over of *p*ABA-related metabolites from the blood meal, 10^7 Berred WT or 10^7 *adcs*$^{-}$ blood stage parasites were injected individually into milk-fed animals. For sporozoite production and subsequent liver stage analysis Berred WT and *adcs*$^{-}$ parasites were also transmitted individually.

Liver Stage Analysis

Analysis of liver stage development *in vitro* was performed with human hepatoma cells (HuH-7, not independently authenticated) which were seeded onto μ-slide 8 well glass bottom slides (Ibidi, Munich, Germany) and inoculated with a mixed population of 5,000 Berred WT and 5,000 *adcs*$^{-}$ sporozoites at subconfluence. Infected cells were grown at a temperature of 37°C and a CO_2 concentration of 5%. Liver stages were imaged and quantified live 24, 48 and 65 hours after infection.

To assess liver stage development *in vivo* C57BL/6 mice were injected intravenously with 10^4 Berred WT or 10^4 *adcs*$^{-}$ sporozoites. For the measurement of first generation parasitemia peripheral blood was subjected to flow cytometry three days after infection. For the quantification of parasite loads livers were harvested 42 hours after injection and total RNA was extracted using TRIzol reagent (Thermo Fisher Scientific). cDNA was synthesized from 1 μg of total RNA with the RETROscript kit (Thermo Fisher Scientific) and quantitative PCR was performed with StepOnePlus (Thermo Fisher Scientific) using Power SYBR Green PCR Master Mix (Thermo Fisher Scientific). The assay was performed in triplicate using primers against mouse *GAPDH* and parasite *18S rRNA* (Table S1; Friesen et al., 2010).

QUANTIFICATION AND STATISTICAL ANALYSIS

Growth curves were analyzed with an ANCOVA. Values > 1% were excluded to restrict analysis to the exponential growth phase. During competitive life cycle progression mutant and WT were compared with a paired t test, comparisons between supplemented and non-supplemented conditions were analyzed with a Student's t test. For comparison of multiple independent experimental conditions, a one-way ANOVA was used in combination with Tukey's multiple comparison test. Time to blood stage patency was analyzed with a Mantel-Cox test. All statistical testing was performed with Prism (version 5.03, GraphPad Software, La Jolla, CA, USA). Effects with P values smaller than 0.05 were considered significant. Statistical details can be found in the corresponding Figure legends.